Geophysical Research Letters

RESEARCH LETTER
10.1029/2019GL085572

Causes and Climatic Consequences of the Impact Winter at the Cretaceous-Paleogene Boundary

Clay R. Tabor[1], Charles G. Bardeen[2], Bette L. Otto-Bliesner[3], Rolando R. Garcia[2], and Owen B. Toon[4]

[1]Department of Geosciences, University of Connecticut, Storrs, CT, USA, [2]Atmospheric Chemistry, Observations and Modeling Laboratory, National Center for Atmospheric Research, Boulder, CO, USA, [3]Climate and Global Dynamics Laboratory, National Center for Atmospheric Research, Boulder, CO, USA, [4]Laboratory for Atmospheric and Space Physics, University of Colorado, Boulder, CO, USA

Key Points:
- Compared to sulfur and dust, soot emission from fires produces the largest reduction in surface light, temperature, and precipitation
- A prolonged reduction in surface light from soot emission could help explain the marine extinction by starvation
- High-latitude coastal regions experienced the least climatic, and likely biotic, disruption from the impact winter

Supporting Information:
- Supporting Information S1

Correspondence to:
C. R. Tabor,
clay.tabor@uconn.edu

Citation:
Tabor, C. R., Bardeen, C. G., Otto-Bliesner, B. L., Garcia, R. R., & Toon, O. B. (2020). Causes and climatic consequences of the impact winter at the Cretaceous-Paleogene boundary. *Geophysical Research Letters*, *47*, e60121. https://doi.org/10.1029/2019GL085572

Received 25 SEP 2019
Accepted 7 JAN 2020
Accepted article online 15 JAN 2020

Abstract Prolonged periods of low light and cold temperatures at Earth's surface are hypothesized effects of the end-Cretaceous asteroid impact. However, debate remains about the causes and consequences of this "impact winter." We perform simulations of the Chicxulub impact with an Earth system model that can simulate the evolution of extreme aerosol loading to quantify the climatic responses to emissions (soot, sulfur, and dust) associated with the impact winter. We show that all impact winter emissions can drastically reduce surface temperature and precipitation. However, only soot emission from impact-driven firestorms is capable of reducing light to below the photosynthetic threshold for many months. Therefore, our results suggest that widespread fires may have been necessary to produce the observed pattern of marine extinction across the Cretaceous-Paleogene boundary. We identify polar coasts and the surrounding open oceans as regions likely to have experienced the least climatic, and biotic, disruption from the impact winter.

Plain Language Summary Over 75% of all species went extinct across the Cretaceous-Paleogene boundary (66 million years ago). This extinction coincided with a massive asteroid impact in the Yucatan Peninsula, which emitted material high into the atmosphere and potentially caused widespread fires. These emissions from the impactor, impact site, and fires would have blocked sunlight from reaching the surface, resulting in an "impact winter" that likely contributed to the mass extinction. However, details of the impact winter have been difficult to quantify. Here we use a state-of-the-art Earth system model to simulate the climate responses to emission of dust and sulfur from the asteroid impact and soot from fires. We find that all simulated emission scenarios reduce sunlight at the surface, cause global cooling, and disrupt the hydrologic cycle. However, only soot emission from fires is able to reduce sunlight, and therefore prevent the growth of primary producers, for long enough to potentially starve large marine organisms. Our results suggest that widespread fires and the resulting soot emission may have been an important component of the extinction. Further, in all emission scenarios we find that the impact winter was least disruptive to the climate in the high-latitude regions, potentially providing refugia for life.

1. Introduction

About 66 million years ago, a massive asteroid (Alvarez et al., 1980; Smit & Hertogen, 1980; Renne et al., 2013) struck the Yucatan Peninsula (Hildebrand et al., 1991), likely leading to an aerosol-driven impact winter (Milne et al., 1982; Toon et al., 1982; Vellekoop et al., 2014, 2016) that contributed to the abrupt disappearance of over 75% of all species across the Cretaceous-Paleogene boundary (KPB) (Jablonski, 1994; Alroy, 2008; Barnosky et al., 2011). Theory, simulations, and observations support a series of postcollision events that rapidly drove Earth into this impact winter state. First, simulations suggest that the energy of impact, along with the composition of the impactor and impact site, resulted in the injection of enormous quantities of dust, sulfur, and other materials into the upper atmosphere that soon engulfed the globe (Pollack et al., 1983; Sigurdsson et al., 1992; Kring et al., 1996). Then, frictional heating from the deposition of recondensed ejecta caused an infrared radiation pulse capable of starting concurrent widespread fires (Melosh et al., 1990; Kring & Durda, 2002; Goldin & Melosh, 2009; Morgan et al., 2013), which emitted large quantities of soot into the atmosphere (Wolbach et al., 2003; Robertson et al., 2013b; Toon et al., 2016). Although debate about the intensity of the thermal pulse and resulting fires remains (see Belcher, 2009, and references therein; Goldin & Melosh, 2009; Morgan et al., 2013), there are multiple lines of evidence for widespread fires soon

after impact (Wolbach et al., 1988; Ivany & Salawitch, 1993; Wolbach et al., 2003). Individually, emission estimates of dust (Toon et al., 2016) or sulfur (Artemieva et al., 2017) from impact or soot (Wolbach et al., 2003) from fires are sufficient to reduce light at the surface and cause temperatures to plummet (Covey et al., 1994; Bardeen et al., 2017; Brugger et al., 2017). However, the magnitude of climate change, regional variability in response, and time scale of recovery resulting from these impact winter emissions remain unclear. Here we address these uncertainties using a complex high-top atmosphere Earth system model configured with an explicit aerosol resolving scheme and Maastrichtian boundary conditions to determine the climatological effects of the most probable drivers of the KPB impact winter: soot, sulfur, and dust.

2. Methods

We perform all experiments with a fully coupled configuration of the Community Earth System Model (CESM) (Gent et al., 2011; Hurrell et al., 2013). This model is able to accurately simulate present-day climate and has been widely used for paleoclimate applications (Brady et al., 2013; Feng et al., 2017). For the atmospheric component of CESM, we use the Whole Atmosphere Community Climate Model (WACCM4), which is a high-top model with an upper boundary at ~140 km and interactive chemistry (Marsh et al., 2013). Within WACCM4, we implement the Community Aerosol and Radiation Model for Atmospheres (CARMA) for explicit aerosol calculations (Toon et al., 1988; Bardeen et al., 2008). Our model configuration accounts for the advection, wet and dry deposition, and radiative effects of aerosols, and allows the aerosol size distribution to evolve freely (Bardeen et al., 2017). We modify the model to reflect late Maastrichtian climate conditions, including period-appropriate CO_2 (560 ppm), paleogeography, and solar irradiance (~1,357 Wm^{-2}) (Tabor et al., 2016). All WACCM4 simulations are initialized from a previously equilibrated Maastrichtian simulation.

We consider soot, SO_2, and dust emissions in isolation and separate impact winter emission types into three categories: fire emissions injected over land surfaces at the local tropopause, ballistic emissions injected globally at 50 km, and splashed emissions injected uniformly above the tropopause around the impact site (Toon et al., 2016). We assume that all soot originates from fires produced by the postimpact infrared thermal pulse. Our emission of 72,700 Tg of carbon from the global fires with 28.6% of that total emitted as fine soot come from measurements of elemental carbon found in KPB clays (Wolbach et al., 1990, 2003). We include emissions of SO_2 from fire, ballistic, and splashed sources (Toon et al., 2016), with the vast majority of the SO_2 coming from the impact site according to the calculations by (Artemieva et al., 2017), who estimate an emission of 325,000 Tg of sulfur, equivalent to 650,000 Tg of SO_2. We also perform a nanoparticles emission scenario based on iron-rich particles found in the global iridium layer (Wdowiak et al., 2001; Ferrow et al., 2011). Based on recent estimates of the impactor and impact site, we inject 2,000,000 Tg of this "dust" ballistically (Toon et al., 2016). We run all impact emission scenarios for 20 years, long enough for the return of surface shortwave radiation (SSWR) to preimpact levels, and compare impact responses with a 30-year WACCM4 Maastrichtian climatology (please refer to the supporting information for additional details about the Earth system model, the boundary conditions, and the asteroid impact emissions).

3. Results

3.1. Shortwave Radiation Response

The most devastating marine kill mechanism associated with the KPB impact winter might have been the reduction in SSWR, not the ensuing cold (Toon et al., 1982; Robertson et al., 2013a). Indeed, there is a well-documented loss of both terrestrial and marine photosynthesizers across the KPB, which suggests that surface light levels were low enough for long enough to cause die-off (Sheehan & Hansen, 1986; Arthur et al., 1987; Vajda & McLoughlin, 2004). In all of our simulated emission scenarios, the flux of SSWR decreases substantially. However, we find that the magnitude and duration of SSWR reduction varies significantly with aerosol type.

Of the three aerosols explored (soot, sulfates, and dust), soot emission results in the largest overall impact on SSWR (Figures 1 and S1). Injection of soot into the upper troposphere and lower stratosphere absorbs incoming solar radiation, heats the surrounding air, and thereby lofts it into the upper atmosphere (Figures 2 and S2). Simultaneously, the high concentration of soot particles leads to rapid coagulation and deposition, with over 90% removal of fine soot and almost complete removal of coarse soot within the first 5 months. Despite

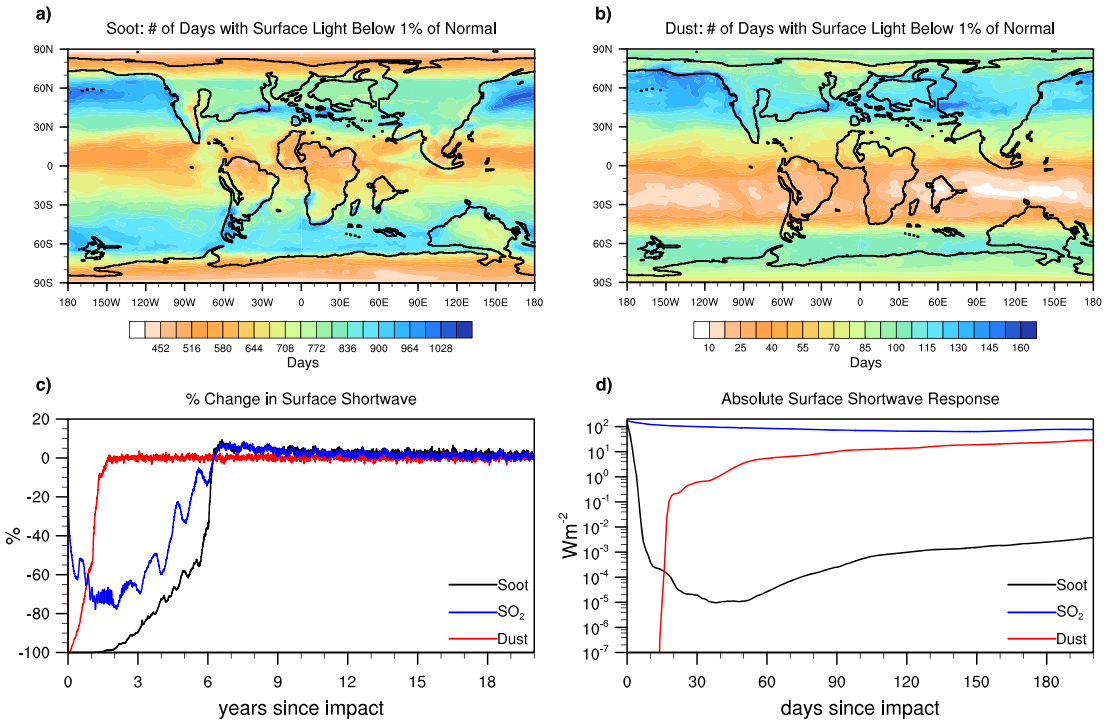

Figure 1. Surface shortwave response to impact aerosols. Number of days with surface shortwave radiation below 1% of climatology after emission of (a) soot and (b) dust. SO_2 emission does not lead to any days with surface shortwave below 1% of normal. Note the difference in scale between contours in (a) and (b). (c) Percent change in global average surface shortwave after aerosol emission relative to climatology. (d) Absolute global average surface shortwave in the first 200 days after aerosol emission.

this, the efficient absorption of shortwave radiation by soot suppresses global SSWR to below the photosynthetic threshold (~1% of normal) (Morel, 1988) for over 20 months; the midlatitudes endure an especially long period of low light conditions. SSWR rapidly recovers at ~70 months post impact due to a feedback involving the reduction of stratospheric heating by thinning soot, which leads to water saturation, condensation, and precipitation (Bardeen et al., 2017) (Figure S2). This process removes the remaining soot, enhanced water vapor, and buildup of low-level clouds from the atmosphere.

Integrated through time since impact, SO_2 emission has the second greatest effect on SSWR (Figures 1 and S1). The high density of SO_2 produces large sulfate particles that, like soot, rapidly settle out of the atmosphere (Figure 2). However, unlike soot, sulfates tend to scatter, instead of absorb, shortwave radiation. In addition, sulfate extinction efficiency decreases as particle size increases, which causes the radiative effect of large SO_2 emissions to be self-limiting (Pinto et al., 1989; Pierazzo et al., 2003). Consequently, sulfate aerosols never reduce SSWR to below the photosynthetic threshold, reaching a global reduction of ~77% of normal (Figure 1). Nevertheless, SO_2 reduces SSWR for over 75 months due to the slow conversion of SO_2 to sulfate. This duration is an upper estimate because we do not include water from the shallow sea impact site (Gulick et al., 2008), which could speed up the conversion from SO_2 to sulfate (Figure S3) (Bekki, 1995), and we do not include emission of SO_3, which may settle out of the atmosphere more rapidly (Pierazzo et al., 2003; Ohno et al., 2014).

Compared to soot and SO_2, dust emission produces the largest absolute reduction in SSWR, with a period of complete darkness, as well as the shortest duration of influence on SSWR, with global flux returning to within 10% of normal after only 17 months (Figures 1 and S1). Although the optical properties of dust vary, it tends to forward scatter and does not absorb radiation as well as soot (Pope, 2002; Hervig et al., 2009). The combination of relatively dense dust particles, rapid coagulation, and limited lofting due to lower absorption of shortwave radiation than soot, results in removal of over 99% of dust mass within 3 months (Figures 2 and S4). While the few weeks of complete darkness from dust would present a unique challenge to life, the

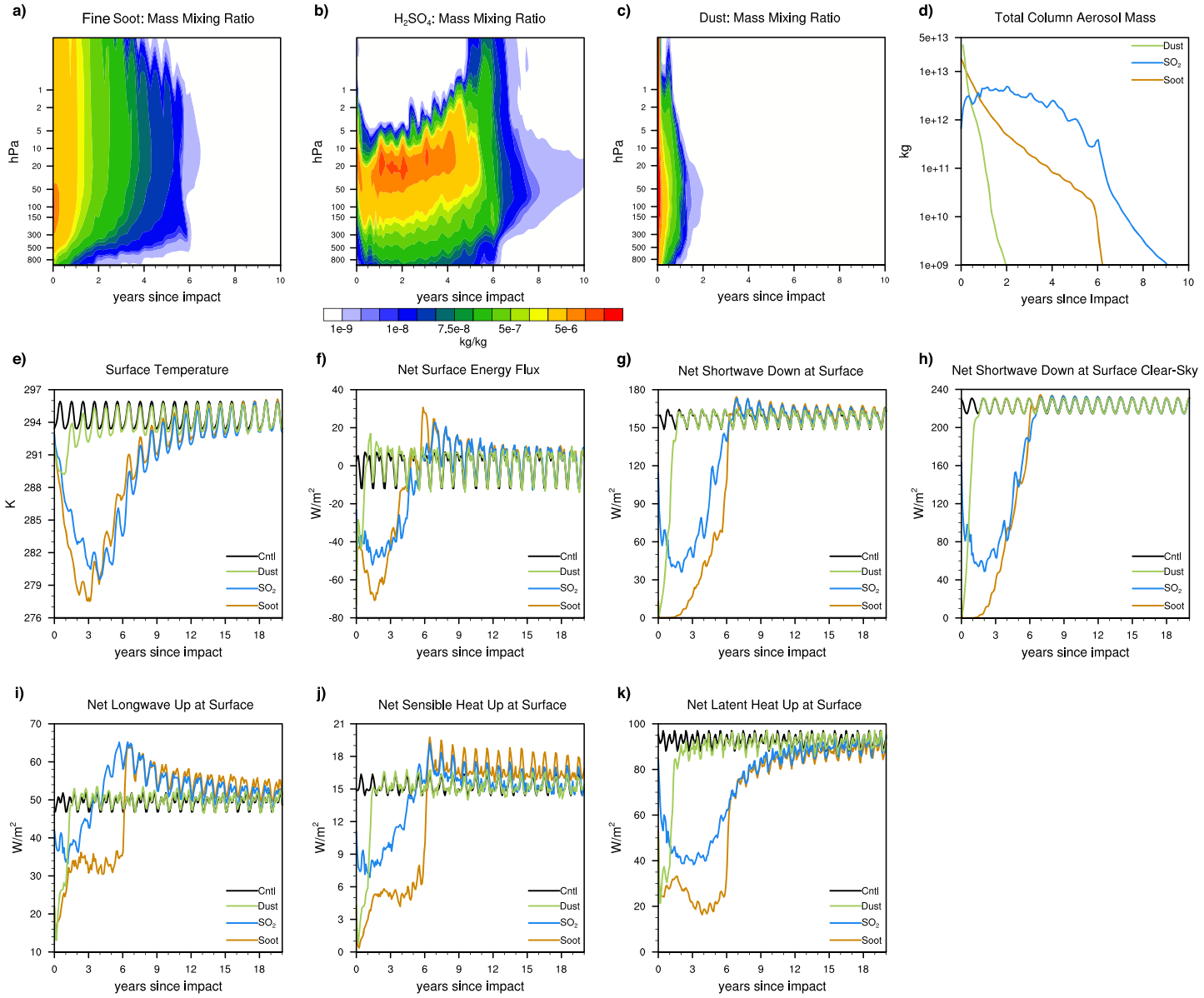

Figure 2. Aerosol concentration and global average surface energy balance changes through time since emission. Global average mass mixing ratio in the atmospheric column through time for (a) fine soot, (b) H_2SO_4, and (c) dust. (d) Total mass of aerosols in the atmosphere through time since emission. Through time since emission, global average (e) surface temperature, (f) net surface energy flux, (g) net shortwave energy flux down at the surface, (h) net shortwave energy flux down at the surface in the absence of clouds, (i) net longwave energy flux up at the surface, (j) net sensible heat flux up at the surface, and (k) net latent heat flux up at the surface. Note that panels (a)–(c) use a nonlinear contouring interval to highlight differences in aerosol response between emission scenarios.

relatively short duration may make this event of secondary significance in the extinction. As a time-integrated quantity over the 20-year simulations, dust reduces SSWR by only 4.9×10^9 J/m^2, while soot and SO_2 reduce SSWR by 2.44×10^{10} and 1.49×10^{10} J/m^2, respectively.

3.2. Temperature Response

The relative warmth of the latest Cretaceous (Upchurch et al., 2015) may have left life on Earth particularly vulnerable to a deep freeze from the impact winter. Despite the overall warmer climate, proxy records show that the meridional temperature and seasonality gradients persisted during the Cretaceous greenhouse (Bowman et al., 2013; O'Brien et al., 2017). Therefore, a strong, long-lasting perturbation in temperature should not affect all ecosystems equally, given that some of the ecosystems could have already been cold

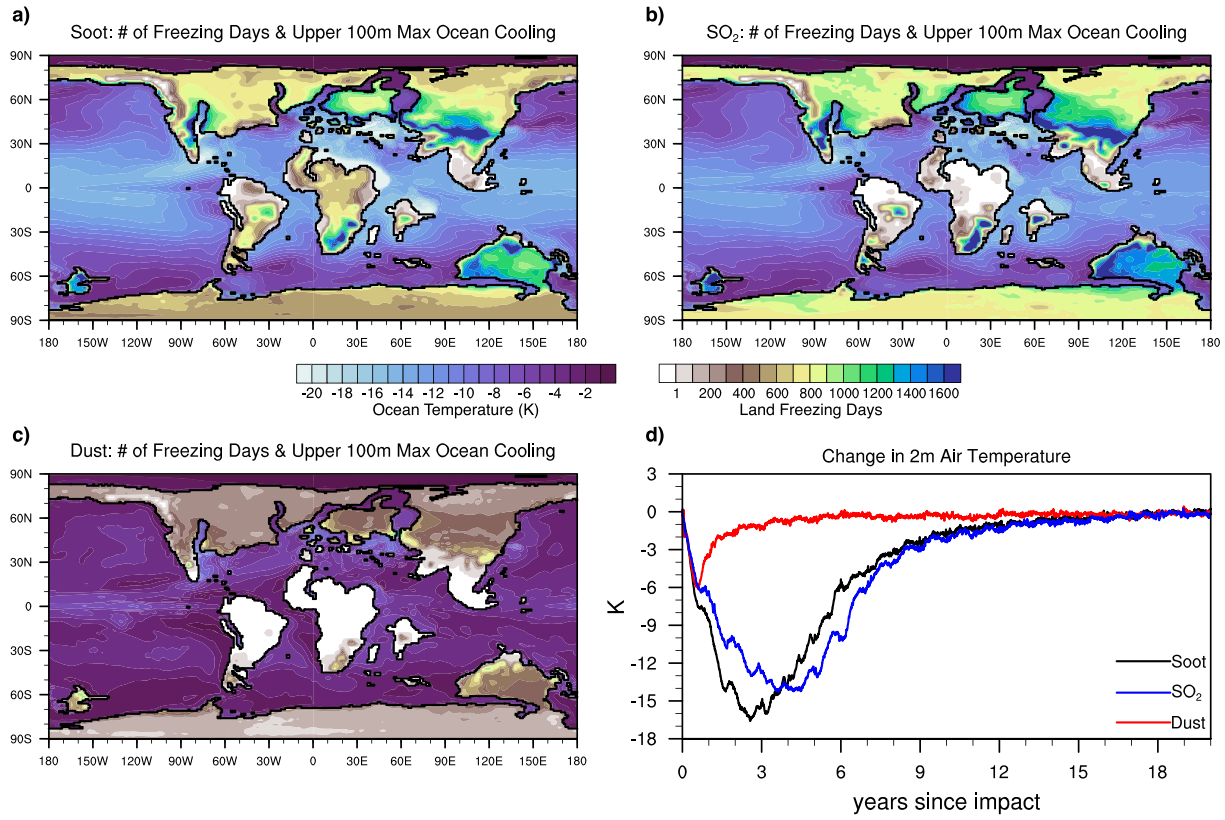

Figure 3. Temperature response to impact aerosols. Maximum cooling in the upper 100 m of the ocean and number of days with below freezing temperatures beyond climatology after emission of (a) soot, (b) SO_2, and (c) dust. (d) Change in global average 2-m air temperature after aerosol emission relative to climatology.

adapted. In our simulations, all emission scenarios cause dramatic surface cooling (Figures 3 and S5). To first order, the magnitude of surface cooling scales with the amount and duration of SSWR change (Figure 2). However, enhanced longwave downwelling from aerosols and clouds, as well as sensible and latent heat reductions, limits surface cooling. In addition, the amount of surface cooling is spatially variable depending on the preimpact climate state and Earth system feedbacks to the aerosol forcing.

Soot emission results in the greatest surface temperature reduction, with maximum global decreases of 29.9 °C after 31 months and 13.2 °C after 38 months for the land and ocean/sea ice surfaces, respectively (Figures 2 and 3). Global surface temperature recovers slowly, to within 1 °C of normal after 138 months. At the ocean surface, soot causes the greatest cooling in equatorial and low-latitude confined seas due mainly to decreased shortwave heating and least cooling in the high-latitude open oceans due to enhanced retention of longwave radiation and increased ocean heat transport associated with extreme deep water formation from cold temperatures and low precipitation (Figure S6). This mixing of cold water to depth results in increased upper-ocean stratification in some regions once sea surface temperatures recover, which may help explain the hypoxic conditions found in the earliest Paleogene (e.g., Galeotti et al., 2004; Vellekoop et al., 2018). Over land, arid regions experience the largest and most rapid cooling, while the thermal inertia of the ocean moderates cooling along many coasts (Figure S5). Many of these large-scale surface temperature changes to soot parallel other simulations that used globally uniform soot emissions, present-day geography and CO_2 (Bardeen et al., 2017), suggesting that Maastrichtian boundary conditions are primarily important for understanding the regional temperature responses to widespread fires.

The global blanket of soot dampens cooling by limiting the escape of longwave into space (Figures 2, 3, and S1). This is especially evident during high-latitude winters in the first few years post impact when high-latitude land surface temperatures are warmer than normal. In addition, heating of surrounding air due to soot creates an inversion, which, in combination with a lack of tropospheric convection, eventually

extends below 700 hPa, trapping water vapor and promoting the formation of low clouds (Figure S2). This response extends the duration of reduced SSWR, latent heat release, and surface longwave radiation (SLWR) loss, and overall lowers the net surface energy deficit.

Although SO_2 injection cools the surface less than does soot, with global maxima on land of 22.4 °C after 43 months and on the ocean/sea ice of 12.0 °C after 49 months, the duration of cooling is slightly longer than that of the soot injection, returning to within 1 °C of climatology after 150 months (Figures 2 and 3). Generally, the spatial and temporal patterns of surface temperature response to SO_2 mimic those of soot. However, SO_2 leads to less cooling over land due a smaller reduction in SSWR (Figures 1 and S5). The high-latitude oceans are the only regions where absolute cooling is greater from SO_2 than from soot, possibly due to slightly weaker ocean heat transport linked to less deep water formation for SO_2 emission (Figure S6).

Like soot, sulfates from SO_2 emission trap much of the longwave radiation. Inclusion of this longwave response may explain the reduced cooling, particularly in the high latitudes, in our simulation relative to another Chicxulub impact SO_2 emission study (Brugger et al., 2017). However, compared with soot, sulfates do not produce a low-level atmospheric inversion and heat the stratosphere less, allowing for greater surface longwave radiation and latent heat loss; maximum global surface cooling from SO_2 is 84% as large as that from soot, even though the total SSWR reduction from SO_2 is only 61% as large as that from soot. Consequently, several midlatitude continents feature a greater increase in the number of freezing days due to SO_2 (Figure 3). Both soot and SO_2 injections show dramatic cooling in the upper ocean near the entrance to the Western Interior Seaway in line with a high-resolution temperature reconstruction across the KPB (Vellekoop et al., 2014).

Dust emission has a moderate effect on surface temperatures relative to soot and SO_2 (Figures 2, 3, and S5). Although dust produces a large surface energy deficit, the short duration of SSWR reduction limits global cooling to 6.4°C after 8 months; many low-latitude regions do not experience freezing. Further, global surface temperature returns to within 1 °C of normal after only 39 months. Given the short duration, the season of dust emission could alter the spatial pattern of cooling.

3.3. Hydrologic Response

Broadly, the aerosol-driven reduction in SSWR decreases convective and baroclinic instabilities in our simulations. For all emission scenarios, low SSWR leads to the rapid breakdown of typical large-scale atmospheric circulation patterns (Figures 4 and S7). The hydrologic cycle subsequently weakens, with greatest precipitation reduction along the Intertropical Convergence Zone (ITCZ). The rapid reduction in precipitation might have been particularly devastating to latest Cretaceous terrestrial life, much of which was accustomed to a moist habitat (Spicer & Herman, 2010). Nevertheless, despite dramatic reductions in precipitation, some regions show moistening of the land mainly as a result of decreased evaporation (Figure S6). The maintenance of soil moisture may have limited desiccation of remaining plant life. This, combined with the prolonged low light conditions, could help explain the fungal and fern spikes in the years after impact (Vajda & McLoughlin, 2004, 2007).

Due to a combination of reduced SSWR and a persistent low-level inversion, both of which lead to less evaporation and convection, soot emission produces a maximum reduction in global precipitation of over 82% after 52 months (Figure 4). Despite this, many previously dry subsidence regions, such as the subtropical oceans and the eastern equatorial Pacific, experience a small increase in precipitation in combination with a large reduction in evaporation, resulting in a period of net moisture surplus. Similarly, high-latitude coasts show a small precipitation increase due to locally strong temperature gradients. However, none of the land surface has enhanced precipitation during reduced SSWR, as cold surface temperatures promote subsidence and offshore flow. In the soot case, an abrupt rebound in precipitation coincides with wet removal of the remaining soot particles after ~70 months (see section 3.1), but the continuation of cool conditions in the tropical Pacific delays complete recovery of the ITCZ for many additional years.

The persistence of moderate levels of SSWR (Figure 1) leads to a less dramatic reduction in the strength of the hydrologic cycle after SO_2 emission relative to soot (Figures 4 and S7). SO_2 causes a maximum reduction in global precipitation of over 58% after 38 months and a recovery to within 10% of normal after 110 months. The continuation of a tropical SSWR maximum allows for the persistence of a weak Hadley circulation, which produces a band of greater precipitation near the equator. Although the spatial patterns of

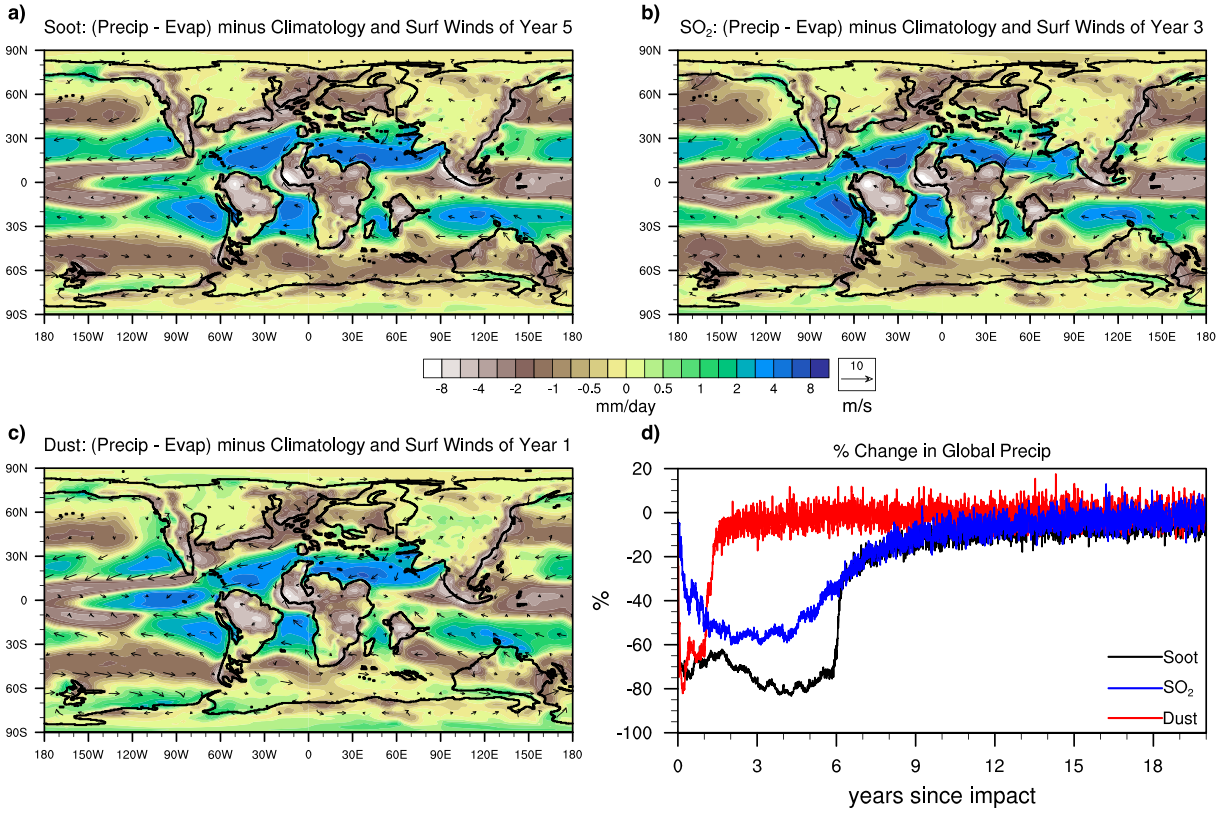

Figure 4. Hydrologic response to impact aerosols. Precipitation minus evaporation and near-surface wind during the year of minimum precipitation after emission of (a) soot, (b) SO_2, and (c) dust. (d) Change in global precipitation after aerosol emission relative to climatology.

hydrologic response are similar for soot and SO_2, lower relative humidity and warmer surface temperatures result in relatively great evaporation and convection in the SO_2 simulation. In particular, compared to soot, SO_2 emission allows for more evaporation over land at low latitudes, which results in greater soil dehydration (Figure S6).

The loss of surface heating from dust emission abruptly weakens tropical convection, decreasing global precipitation by 80% within a few months (Figures 4 and S7). During the relatively short period of low SSWR, moisture budget patterns from dust resemble those of soot and SO_2. However, the rapid return of SSWR results in relatively little lasting effect on ocean temperatures. Therefore, precipitation along the ITCZ is able to recover more quickly, returning to within 10% of normal after only 19 months. Although the magnitude of emission is significantly smaller, Kaiho et al. (2016) show a similar hydrologic response to soot emission in their KPB simulations, suggesting that the large-scale patterns of response to extreme aerosol loading is unlikely to be model dependent.

4. Discussion

Our simulations show that soot emission from widespread fires would probably lead to the greatest biotic hardship, given that it results in the longest duration of SSWR below 1% of normal; greatest overall surface cooling; and largest disruption to the hydrological cycle. Although postimpact burn estimates remain controversial (Belcher, 2009; Morgan et al., 2013), even in our scenarios with less biomass burning, soot still reduces global SSWR, surface temperature, and precipitation more than do SO_2 and dust (Figure S8) (Bardeen et al., 2017). In addition, research suggests that the exceptionally high heat from the global fires would likely consume most organic carbon, limiting the potential for atmospheric residence time uncertainty associated with organic coatings on the soot (Jacobson, 2002).

4.1. Potential for Aerosol Interactions

The greater climatic significance of soot compared to SO_2 and dust emissions is unlikely dependent on our experiment design, which only considers aerosol emissions in isolation. Previous work shows that although the addition of water from the shallow sea impact site is able to wash a portion of the soot out of the atmosphere soon after impact, the longer-term radiative effects remain largely unchanged (Bardeen et al., 2017). In contrast, the addition of water in the SO_2 emission scenario could reduce the radiative effect by increasing the rate of sulfate production (Bekki, 1995), leading to faster coagulation and settling. Thus, soot would likely remain the most consequential impact winter aerosol to the climate in combined emission scenarios.

4.2. Drivers of Extinction

Regardless of aerosol type, it seems unlikely that the observed pattern of marine extinction at the KPB was the result of cooling alone. In our simulations, many high-latitude upper-ocean regions cool by little more than the temperature range across a normal seasonal cycle, and this cooling persists for less than 2 years (Figures 3 and S5). Further, although our experiments are unable to directly address the potential for ocean acidification, the simulated deposition rate and latest sulfur emission estimates do not support the level of undersaturation that other research suggests is necessary to drive extinction of calcifiers (Tyrrell et al., 2015); however, emission of primarily SO_3, instead of SO_2 or the addition of water, could lead to more rapid deposition of sulfates [(Ohno et al., 2014; Bekki, 1995). The ocean also acts as a buffer against the harmful effects of an infrared pulse (Robertson et al., 2004) and, to an extent, excess surface ultraviolet radiation from the potential aerosol-driven loss of stratospheric ozone (Pierazzo et al., 2010). Alternatively, several studies propose a food web collapse triggered by the loss of primary producers (Milne et al., 1982; Sheehan & Hansen, 1986; Arthur et al., 1987; Robertson et al., 2013a). Although the combination of low SSWR and cool upper-ocean temperatures may have limited the habitable range of primary producers, our results show that sulfates from SO_2 emission do not block enough SSWR to prevent photosynthesis, and dust emission does not block SSWR for long enough to cause starvation of the higher trophic levels (Figures 1 and S1). However, soot injection, which blocks over 99% of SSWR for almost 2 years, supports a bottom-up marine ecosystem collapse by way of starvation.

4.3. Refugia

Our model results suggest the polar coasts and surrounding open oceans provide the most probable refugia from the impact winter. Biota in these regions would have been best acclimated to the prolonged night produced by soot emissions, because they survive periods of low SSWR seasonally (Whittle et al., 2019). Furthermore, even though the high-latitude coasts show a moderate increase in the number of freezing days in our simulations, this climate was already cool and seasonal in the latest Cretaceous, with biota conditioned to survive subfreezing temperatures (Figure S5) (Bowman et al., 2013; Tabor et al., 2016). In addition, these regions show some of the smallest postimpact cooling due to a combination of increased ocean heat transport and longwave downwelling by aerosols (Figures 2, 3, and S1). Finally, changes in precipitation and evaporation are relatively minimal in the high latitudes because of limited deep convection and high relative humidity prior to impact, allowing for maintenance of preimpact soil moisture (Figures 4 and S6). In our simulations, these high-latitude temperature and hydrologic changes are largely independent of aerosol forcing, with a similar response to both soot and SO_2 emissions. Therefore, in any impact winter scenario, a relative refuge in the high-latitudes should persist. The potential for improved floral and faunal survival at high latitudes is supported by a variety of fossil records (Vajda & McLoughlin, 2007; Jiang et al., 2010; Donovan et al., 2017; Whittle et al., 2019). Nevertheless, other impact-driven extinction mechanisms, such as proximity to the impact site, cannot be ruled out as the cause of the observed spatial heterogeneity in extinction and recovery. Further, determining the latitude of survival is often biased by spatial disparity in sample density between latitudes and hemispheres (Reddin et al., 2019).

4.4. The Importance of Aerosol Type

Estimates of dust injection from the Chicxulub impact are more poorly constrained than soot and SO_2 (Pope, 2002; Toon et al., 2016). However, this may not be a major limitation for understanding the KPB extinction, because our simulations show that dust has a relatively short atmospheric residence time. Similarly, uncertainties in emission magnitudes of soot (Wolbach et al., 2003) and SO_2 (Artemieva et al., 2017) might be of secondary importance since, as we and others show, their radiative effects saturate at high concentrations

(Pinto et al., 1989; Bardeen et al., 2017). In contrast, our results highlight the importance of particle type to the climate response. Although both soot and SO_2 emissions produce a prolonged impact winter with severe cooling over land in our simulations, only soot prevents photosynthetic activity for a long enough period to cause starvation of the high trophic levels. Because cooling alone from these impact winter emission scenarios seems insufficient to cause extinction in many regions of the ocean, the sustained reduction in light from soot emission may best explain the pattern of marine biotic response, providing additional support for widespread fires after the Chicxulub impact.

Acknowledgments
AcknowledgementsWe would like to acknowledge Johan Vellekoop, Natalia Artemieva, and anonymous reviewers, whose comments improved the quality of this manuscript. Clay Tabor acknowledges funding from the National Center for Atmosphere Research Advanced Study Program postdoctoral fellowship. The CESM project is supported primarily by the National Science Foundation (NSF). This material is based upon work supported by the National Center for Atmospheric Research, which is a major facility sponsored by the NSF under Cooperative Agreement 1852977. Computing and data storage resources, including the Cheyenne supercomputer (doi:10.5065/D6RX99HX), were provided by the Computational and Information Systems Laboratory (CISL) at NCAR. The monthly atmospheric model data presented in this manuscript are available on https://www.pangaea.de (see data citation Tabor et al., 2020). Additional simulation data associated with these experiments are stored publicly on the NCAR Campaign Storage file system (https://www2.cisl.ucar.edu/resources/storage-and-file-systems/campaign-storage-file-system) at /gpfs/csfs1/cesm/development/palwg/Tabor_paleo/KPB_GRL.

References

Alroy, J. (2008). Dynamics of origination and extinction in the marine fossil record, Proceedings of the National Academy of Sciences.
Alvarez, L. W., Alvarez, W., Asaro, F., & Michel, H. V. (1980). Extraterrestrial cause for the Cretaceous-Tertiary extinction. *Science*, *208*(4448), 1095–1108. https://doi.org/10.1126/science.208.4448.1095
Artemieva, N., Morgan, J., & E. 3. S. Party (2017). Quantifying the release of climate-active gases by large meteorite impacts with a case study of Chicxulub. *Geophysical Research Letters*, *44*(20), 10–180–10–188.
Arthur, M. A., Zachos, J. C., & Jones, D. S. (1987). Primary productivity and the Cretaceous/Tertiary boundary event in the oceans. *Cretaceous Research*, *8*(1), 43–54.
Bardeen, C. G., Garcia, R. R., Toon, O. B., & Conley, A. J. (2017). On transient climate change at the Cretaceous–Paleogene boundary due to atmospheric soot injections. *Proceedings of the National Academy of Sciences*, *114*(36), E7415–E7424.
Bardeen, C. G., Toon, O. B., Jensen, E. J., Marsh, D. R., & Harvey, V. L. (2008). Numerical simulations of the three-dimensional distribution of meteoric dust in the mesosphere and upper stratosphere. *Journal of Geophysical Research-Atmospheres*, *113*(D17), D17202. https://doi.org/10.1029/2007JD009515
Barnosky, A. D., Matzke, N., Tomiya, S., Wogan, G. O., Swartz, B., Quental, T. B., et al. (2011). Has the Earth's sixth mass extinction already arrived? *Nature*, *471*(7336), 51–57. https://doi.org/10.1038/nature09678
Bekki, S. (1995). Oxidation of volcanic SO_2: A sink for stratospheric OH and H_2O. *Geophysical Research Letters*, *22*(8), 913–916.
Belcher, C. M. (2009). Reigniting the Cretaceous-Palaeogene firestorm debate. *Geology*, *37*(12), 1147–1148.
Bowman, V. C., Francis, J. E., & Riding, J. B. (2013). Late Cretaceous winter sea ice in Antarctica? *Geology*, *41*(12), 1227–1230.
Brady, E. C., Otto-Bliesner, B. L., Kay, J. E., & Rosenbloom, N. (2013). Sensitivity to glacial forcing in the CCSM4. *Journal of Climate*, *26*(6), 1901–1925.
Brugger, J., Feulner, G., & Petri, S. (2017). Baby, it's cold outside: Climate model simulations of the effects of the asteroid impact at the end of the Cretaceous. *Geophysical Research Letters*, *44*(1), 419–427.
Covey, C., Thompson, S. L., Weissman, P. R., & MacCracken, M. C. (1994). Global climatic effects of atmospheric dust from an asteroid or comet impact on Earth. *Global and Planetary Change*, *9*(3-4), 263–273.
Donovan, M. P., Iglesias, A., Wilf, P., Labandeira, C. C., & Cúneo, N. R. (2017). Rapid recovery of Patagonian plant–insect associations after the end-Cretaceous extinction. *Nature Ecology & Evolution*, *1*(1), 0012.
Feng, R., Otto-Bliesner, B. L., Fletcher, T. L., Tabor, C. R., Ballantyne, A. P., & Brady, E. C. (2017). Amplified Late Pliocene terrestrial warmth in northern high latitudes from greater radiative forcing and closed Arctic Ocean gateways. *Earth and Planetary Science Letters*, *466*, 129–138.
Ferrow, E., Vajda, V., Koch, C. B., Peucker-Ehrenbrink, B., & Willumsen, P. S. (2011). Multiproxy analysis of a new terrestrial and a marine Cretaceous–Paleogene (K–Pg) boundary site from New Zealand. *Geochimica et Cosmochimica Acta*, *75*(2), 657–672.
Galeotti, S., Brinkhuis, H., & Huber, M. (2004). Records of post–Cretaceous-Tertiary boundary millennial-scale cooling from the western Tethys: A smoking gun for the impact-winter hypothesis? *Geology*, *32*(6), 529–532.
Gent, P. R., Danabasoglu, G., Donner, L. J., Holland, M. M., Hunke, E. C., Jayne, S. R., et al. (2011). The community climate system model version 4. *Journal of Climate*, *24*(19), 4973–4991.
Goldin, T. J., & Melosh, H. J. (2009). Self-shielding of thermal radiation by Chicxulub impact ejecta: Firestorm or fizzle? *Geology*, *37*(12), 1135–1138.
Gulick, S. P., Barton, P. J., Christeson, G. L., Morgan, J. V., McDonald, M., Mendoza-Cervantes, K., et al. (2008). Importance of pre-impact crustal structure for the asymmetry of the Chicxulub impact crater. *Nature Geoscience*, *1*(2), 131.
Hervig, M. E., Gordley, L. L., Deaver, L. E., Siskind, D. E., Stevens, M. H., Russell, J. M., et al. (2009). First satellite observations of meteoric smoke in the middle atmosphere. *Geophysical Research Letters*, *36*(18), L18805. https://doi.org/10.1029/2009GL039737
Hildebrand, A. R., Penfield, G. T., Kring, D. A., Pilkington, M., Camargo, Z. A., Jacobsen, S. B., & Boynton, W. V. (1991). Chicxulub crater: A possible Cretaceous/Tertiary boundary impact crater on the Yucatan Peninsula, Mexico. *Geology*, *19*(9), 867–871.
Hurrell, J. W., Holland, M. M., Gent, P. R., Ghan, S., Kay, J. E., Kushner, P. J., et al. (2013). The community earth system model: A framework for collaborative research. *Bulletin of the American Meteorological Society*, *94*(9), 1339–1360.
Ivany, L. C., & Salawitch, R. J. (1993). Carbon isotopic evidence for biomass burning at the KT boundary. *Geology*, *21*(6), 487–490.
Jablonski, D. (1994). Extinctions in the fossil record. *Phil. Trans. R. Soc. Lond. B*, *344*(1307), 11–17.
Jacobson, M. Z. (2002). Control of fossil-fuel particulate black carbon and organic matter, possibly the most effective method of slowing global warming. *Journal of Geophysical Research, Planets*, *107*(D19), ACH 16–1–ACH 16–22.
Jiang, S., Bralower, T. J., Patzkowsky, M. E., Kump, L. R., & Schueth, J. D. (2010). Geographic controls on nannoplankton extinction across the Cretaceous/Palaeogene boundary. *Nature Geoscience*, *3*(4), 280.
Kring, D. A., & Durda, D. D. (2002). Trajectories and distribution of material ejected from the Chicxulub impact crater: Implications for postimpact wildfires. *Journal of Geophysical Research, Planets*, *107*(E8), 6–1–6–22.
Kring, D. A., Melosh, H. J., & Hunten, D. M. (1996). Impact-induced perturbations of atmospheric sulfur. *Earth and Planetary Science Letters*, *140*(1-4), 201–212.
Marsh, D. R., Mills, M. J., Kinnison, D. E., Lamarque, J.-F., Calvo, N., & Polvani, L. M. (2013). Climate change from 1850 to 2005 simulated in CESM1 (WACCM). *Journal of Climate*, *26*(19), 7372–7391.
Melosh, H. J., Schneider, N. M., Zahnle, K. J., & Latham, D. (1990). Ignition of global wildfires at the Cretaceous/Tertiary boundary. *Nature*, *343*(6255), 251–254. https://doi.org/10.1038/343251a0

Milne, D. H., McKay, C. P., Silver, L. T., & Schultz, P. H. (1982). Response of marine plankton communities to a global atmospheric darkening. *Geological implications of impacts of large asteroids and comets on the Earth*, *190*, 297–303.
Morel, A. (1988). Optical modeling of the upper ocean in relation to its biogenous matter content (case I waters). *Journal of Geophysical Research-Atmospheres*, *93*(C9), 10749–10768.
Morgan, J., Artemieva, N., & Goldin, T. (2013). Revisiting wildfires at the K-Pg boundary. *Journal of Geophysical Research – Biogeosciences*, *118*(4), 1508–1520.
O'Brien, C. L., Robinson, S. A., Pancost, R. D., Damsté, J. S. S., Schouten, S., Lunt, D. J., et al. (2017). Cretaceous sea-surface temperature evolution: Constraints from TEX86 and planktonic foraminiferal oxygen isotopes. *Earth-Science Reviews*, *172*, 224–247.
Ohno, S., Kadono, T., Kurosawa, K., Hamura, T., Sakaiya, T., Shigemori, K., et al. (2014). Production of sulphate-rich vapour during the Chicxulub impact and implications for ocean acidification. *Nature Geoscience*, *7*(4), 279.
Pierazzo, E., Garcia, R. R., Kinnison, D. E., Marsh, D. R., Lee-Taylor, J., & Crutzen, P. J. (2010). Ozone perturbation from medium-size asteroid impacts in the ocean. *Earth and Planetary Science Letters*, *299*(3-4), 263–272.
Pierazzo, E., Hahmann, A. N., & Sloan, L. C. (2003). Chicxulub and climate: Radiative perturbations of impact-produced S-bearing gases. *Astrobiology*, *3*(1), 99–118. https://doi.org/10.1089/153110703321632453
Pinto, J. P., Turco, R. P., & Toon, O. B. (1989). Self-limiting physical and chemical effects in volcanic eruption clouds. *Journal of Geophysical Research-Atmospheres*, *94*(D8), 11,165–11,174.
Pollack, J. B., Toon, O. B., Ackerman, T. P., McKay, C. P., & Turco, R. P. (1983). Environmental effects of an impact-generated dust cloud: implications for the Cretaceous-Tertiary extinctions. *Science*, *219*(4582), 287–289. https://doi.org/10.1126/science.219.4582.287
Pope, K. O. (2002). Impact dust not the cause of the Cretaceous-Tertiary mass extinction. *Geology*, *30*(2), 99–102.
Reddin, C. J., Kocsis, Á. T., & Kiessling, W. (2019). Climate change and the latitudinal selectivity of ancient marine extinctions. *Paleobiology*, *45*(1), 70–84.
Renne, P. R., Deino, A. L., Hilgen, F. J., Kuiper, K. F., Mark, D. F., Mitchell, W. S., et al. (2013). Time scales of critical events around the Cretaceous-Paleogene boundary. *Science*, *339*(6120), 684–687. https://doi.org/10.1126/science.1230492
Robertson, D. S., Lewis, W. M., Sheehan, P. M., & Toon, O. B. (2013a). K-Pg extinction patterns in marine and freshwater environments: The impact winter model. *Journal of Geophysical Research – Biogeosciences*, *118*(3), 1006–1014.
Robertson, D. S., Lewis, W. M., Sheehan, P. M., & Toon, O. B. (2013b). K-Pg extinction: Reevaluation of the heat-fire hypothesis. *Journal of Geophysical Research – Biogeosciences*, *118*(1), 329–336.
Robertson, D. S., McKenna, M. C., Toon, O. B., Hope, S., & Lillegraven, J. A. (2004). Survival in the first hours of the Cenozoic. *Geological Society of America Bulletin*, *116*(5-6), 760–768.
Sheehan, P. M., & Hansen, T. A. (1986). Detritus feeding as a buffer to extinction at the end of the Cretaceous. *Geology*, *14*(10), 868–870.
Sigurdsson, H., D'Hondt, S., & Carey, S. (1992). The impact of the Cretaceous/Tertiary bolide on evaporite terrane and generation of major sulfuric acid aerosol. *Earth and Planetary Science Letters*, *109*(3-4), 543–559.
Smit, J., & Hertogen, J. (1980). An extraterrestrial event at the Cretaceous–Tertiary boundary. *Nature*, *285*(5762), 198.
Spicer, R. A., & Herman, A. B. (2010). The Late Cretaceous environment of the Arctic: A quantitative reassessment based on plant fossils, Palaeogeography, Palaeoclimatology. *Palaeoecology*, *295*(3-4), 423–442.
Tabor, C. R., Bardeen, C., Otto-Bliesner, B., Garcia, R., & Toon, O. (2020). Simulations of the Impact Winter at the Cretaceous-Paleogene Boundary. PANGAEA. https://doi.org/10.1594/PANGAEA.909529
Tabor, C. R., Poulsen, C. J., Lunt, D. J., Rosenbloom, N. A., Otto-Bliesner, B. L., Markwick, P. J., et al. (2016). The cause of Late Cretaceous cooling: A multimodel-proxy comparison. *Geology*, *44*(11), 963–966.
Toon, O. B., Bardeen, C., & Garcia, R. (2016). Designing global climate and atmospheric chemistry simulations for 1 and 10 km diameter asteroid impacts using the properties of ejecta from the K-Pg impact. *Atmospheric Chemistry and Physics*, *16*(20), 13,185–13,212.
Toon, O. B., Pollack, J. B., Ackerman, T. P., Turco, R. P., Mckay, C. P., & Liu, M. S. (1982). Evolution of an impact-generated dust cloud and its effects on the atmosphere.
Toon, O. B., Turco, R. P., Westphal, D., Malone, R., & Liu, M. (1988). A multidimensional model for aerosols: Description of computational analogs. *Journal of the Atmospheric Sciences*, *45*(15), 2123–2144.
Tyrrell, T., Merico, A., & McKay, D. I. A. (2015). Severity of ocean acidification following the end-Cretaceous asteroid impact. *Proceedings of the National Academy of Sciences*, *112*(21), 6556–6561. 201418604
Upchurch, G. R. Jr., Kiehl, J., Shields, C., Scherer, J., & Scotese, C. (2015). Latitudinal temperature gradients and high-latitude temperatures during the latest Cretaceous: Congruence of geologic data and climate models. *Geology*, *43*(8), 683–686.
Vajda, V., & McLoughlin, S. (2004). Fungal proliferation at the Cretaceous-Tertiary boundary. *Science*, *303*(5663), 1489–1489. https://doi.org/10.1126/science.1093807
Vajda, V., & McLoughlin, S. (2007). Extinction and recovery patterns of the vegetation across the Cretaceous–Palaeogene boundary—A tool for unravelling the causes of the end-Permian mass-extinction. *Review of Palaeobotany and Palynology*, *144*(1-2), 99–112.
Vellekoop, J., Esmeray-Senlet, S., Miller, K. G., Browning, J. V., Sluijs, A., van de Schootbrugge, B., et al. (2016). Evidence for Cretaceous-Paleogene boundary bolide "impact winter" conditions from New Jersey, USA. *Geology*, *44*(8), 619–622.
Vellekoop, J., Sluijs, A., Smit, J., Schouten, S., Weijers, J. W., Damsté, J. S. S., & Brinkhuis, H. (2014). Rapid short-term cooling following the Chicxulub impact at the Cretaceous–Paleogene boundary. *Proceedings of the National Academy of Sciences*, *111*(21), 7537–7541.
Vellekoop, J., Woelders, L., van Helmond, N. A., Galeotti, S., Smit, J., Slomp, C. P., et al. (2018). Shelf hypoxia in response to global warming after the Cretaceous-Paleogene boundary impact. *Geology*, *46*(8), 683–686. https://doi.org/10.1130/G45000.1
Wdowiak, T. J., Armendarez, L. P., Agresti, D. G., Wade, M. L., Wdowiak, S. Y., Claeys, P., & Izett, G. (2001). Presence of an iron-rich nanophase material in the upper layer of the Cretaceous-Tertiary boundary clay. *Meteoritics & Planetary Science*, *36*(1), 123–133.
Whittle, R. J., Witts, J. D., Bowman, V. C., Crame, J. A., Francis, J. E., & Ineson, J. (2019). Nature and timing of biotic recovery in Antarctic benthic marine ecosystems following the Cretaceous–Palaeogene mass extinction. *Palaeontology*, *62*(6), 919–934. https://doi.org/10.1111/pala.12434
Wolbach, W. S., Gilmour, I., & Anders, E. (1990). Major wildfires at the Cretaceous/Tertiary boundary. *Geological Society of America Special Papers*, *247*, 391–400.
Wolbach, W. S., Gilmour, I., Anders, E., Orth, C. J., & Brooks, R. R. (1988). Global fire at the Cretaceous–Tertiary boundary. *Nature*, *334*(6184), 665.
Wolbach, W. S., Widicus, S., & Kyte, F. T. (2003). A search for soot from global wildfires in central Pacific Cretaceous-Tertiary boundary and other extinction and impact horizon sediments. *Astrobiology*, *3*(1), 91–97. https://doi.org/10.1089/153110703321632444